Article

Detection and Analysis of Corrosion on Coated Metal Surfaces Using Enhanced YOLO v5 Algorithm for Anti-Corrosion Performance Evaluation

Qifeng Yu *[ID], Yudong Han, Wuguang Lin and Xinjia Gao[ID]

College of Transport and Communications, Shanghai Maritime University, Shanghai 201306, China;
202330610077@stu.shmtu.edu.cn (Y.H.); wglin@shmtu.edu.cn (W.L.); xjgao@shmtu.edu.cn (X.G.)
* Correspondence: qfyu@shmtu.edu.cn

Abstract: This study addresses the severe corrosion issues in the coastal regions of southern China by proposing an improved YOLO v5-GOLD-NWD model. Utilizing corrosion data from the National Center for Materials Corrosion and Protection Science of China, a dataset was constructed for metal-surface corrosion under different protective coatings. This dataset was used for model training, testing, and comparison. Model accuracy was validated using precision, recall, F1 score, and prediction probability. The results demonstrate that the proposed improved model exhibits better identification precision in metal corrosion detection, achieving 78%, a 4% improvement compared to traditional YOLO v5 models. Additionally, through identification and statistical analysis of corrosion image datasets from five types of coated metal specimens, it was found that powder epoxy coating, fluorocarbon coating, epoxy coating, and chlorinated rubber coating showed good corrosion resistance after 24 months of exposure. Conversely, Wuxi anti-fouling coating exhibited poor corrosion resistance. After 60 months of natural exposure, the powder epoxy coating specimens had the highest corrosion occurrence probability, followed by chlorinated rubber coating and epoxy coating, with fluorocarbon coating showing relatively lower probability. The fluorocarbon coating demonstrated relatively good corrosion resistance at both 24 and 60 months of exposure. The findings of this study provide a theoretical basis for enhancing the corrosion protection effectiveness of steel structures in coastal areas.

Keywords: metal corrosion; YOLO v5; machine vision technology; corrosion coatings; marine environmental corrosion

1. Introduction

In coastal marine areas, engineering infrastructure typically faces more severe corrosion issues, primarily due to the presence of salt and other corrosive substances in seawater. These accelerate the corrosion rate of construction materials, especially metals, leading to significant functional losses in many engineering infrastructures. This not only threatens the performance and service life of equipment but also poses potential hazards to the safety of personnel and the environment [1]. Corrosion-induced equipment damage, toxic substance leakage, fires, explosions, and other catastrophic events result in immeasurable losses to society [2]. Therefore, corrosion identification, detection, and protection in marine and coastal engineering infrastructure have always been focal points of concern for relevant personnel [3].

Traditional methods for corrosion detection and identification in marine and coastal engineering infrastructure mainly include visual inspection, physical testing, chemical testing, electrochemical testing, non-destructive testing (such as ultrasonic, X-ray, magnetic particle inspection, etc.), infrared thermography, fiber optic sensing, and remote sensing technology [4,5]. With the development of artificial intelligence technology, data-driven intelligent monitoring techniques are gradually being applied to corrosion detection and

monitoring in marine and coastal engineering infrastructure. Through real-time monitoring and data analysis, it enables timely identification and warning of corrosion issues [6–8]. In emerging intelligent detection technologies, image processing, computer vision, and machine learning methods are widely used for processing corrosion monitoring images, extracting features, detecting targets, identifying corrosion patterns, classifying, and predicting. This enables automated monitoring and detection of corrosion issues, improving monitoring efficiency and accuracy, and providing important support for engineering management and maintenance [9–12].

In corrosion detection, image processing techniques can visualize corrosion by segmenting, filtering, sharpening, and enhancing corrosion areas in images [9]. Many scholars have developed different image recognition techniques for detecting corrosion areas based on image processing technology, such as color space detection [12,13], corrosion area computation [14], corrosion area classification [15], surface feature change analysis, etc. [16,17]. Through image processing technology, corrosion areas can be identified and classified more accurately, providing important information for corrosion assessment. Machine learning is a branch of artificial intelligence that involves algorithms and statistical models. By training on datasets, it identifies patterns and makes predictions or decisions, enabling computer systems to learn from data and improve their performance [18,19]. Computer vision focuses on developing algorithms and technologies to extract high-level semantic feature information from images using image processing techniques and utilize these features for tasks such as object recognition, detection, and classification. Machine vision relies on image processing to provide clear image data and depends on machine learning algorithms, especially deep learning, to enhance the understanding and analysis of image content [20]. Therefore, many scholars apply machine learning to the detection and evaluation of corrosion processes [21–23]. Common machine learning methods include artificial neural network models, random forest models, support vector machine models, etc. [24,25].

Neural network models in corrosion research include Back-propagation (BP) Networks [26,27], Radial Basis Function (RBF) Networks [28–30], Deep Neural Networks (DNNs) [31,32], and Convolutional Neural Networks (CNNs) [7,21,33,34]. BP and RBF networks model complex relationships between environmental and material parameters and corrosion rates using historical data, enabling accurate predictions and multi-factor analysis [26,27,35,36]. BP networks, however, suffer from long training times and overfitting, while RBF networks outperform in prediction accuracy and speed but depend heavily on the selection of radial basis function centers and training data quality [24]. Optimization algorithms and hybrid models have been used to enhance RBF performance [37,38]. DNNs, with their multiple hidden layers, excel in learning complex patterns for tasks such as predicting corrosion rates, classifying images, and detecting corrosion [31,32,39,40]. Despite their high computational costs and overfitting risks, DNNs require large datasets and manually designed feature extractors. CNNs are ideal for image data, extracting features for classification and detection tasks, and are widely used in corrosion morphology identification [21–23,41–43]. However, CNNs cannot correlate material corrosion with environmental factors, limiting their predictive capabilities in specific environments [24,32].

The Random Forest (RF) model is an ensemble learning algorithm that constructs multiple decision trees for classification or regression predictions. It has good generalization ability, can handle high-dimensional data, and is resistant to overfitting while being capable of parallel processing. Consequently, it is widely applied in corrosion research, including corrosion rate prediction [44–47], environmental factor analysis [47,48], and corrosion type identification [49]. The RF model is suitable for complex corrosion prediction tasks but may have lower accuracy with small sample sizes or datasets with fewer features. Additionally, it requires significant computational resources and has less interpretability compared to traditional statistical methods. Support Vector Machine (SVM) is a supervised learning algorithm primarily used for classification but also applicable to regression (Support Vector Regression, SVR). SVM overcomes issues like slow convergence, the need for large datasets,

and overfitting, making it useful for corrosion prediction [50–52] and corrosion performance assessment [53]. SVM models are relatively interpretable, aiding in understanding the impact of different factors on corrosion behavior. However, SVM may face computational efficiency issues with large datasets, and selecting an appropriate kernel function for nonlinear problems can be challenging.

With the development of machine learning and computer vision technologies, Redmon et al. [54] introduced the YOLO (You Only Look Once) object detection algorithm. Unlike traditional two-stage detection algorithms like the R-CNN series, YOLO simultaneously predicts bounding boxes, class probabilities, and object positions in a single image processing stage. By transforming object detection into a regression problem, YOLO achieves fast detection by directly mapping image pixels to bounding box coordinates through deep neural networks. Its rapid detection capability and end-to-end nature make it widely applicable in corrosion detection. For example, Jia et al. [55] developed the Corrosion-YOLO v5s model for detecting corrosion in public facilities, demonstrating excellent detection accuracy using a dataset of metal corrosion images. Zhang et al. [56] created an aircraft surface defect detection model based on YOLO, comparing it with Faster R-CNN and introducing SSD (Single-Shot MultiBox Detector) and Mask R-CNN models to analyze aircraft surface defect recognition accuracy. Nabizadeh and Parghi [57] trained YOLO v3, YOLO v5s, and YOLO v7 models on concrete corrosion images, comparing their performance using metrics such as accuracy, F1 score, recall, and mean Average Precision (mAP). They found YOLO v5s performed best in concrete corrosion detection, providing early warnings to prevent structural failures. Ameli et al. [58] constructed an open-source dataset of steel bridge corrosion with annotations, training and validating Mask R-CNN and YOLO v8 algorithms, which exhibited satisfactory performance in corrosion segmentation and grading.

In conclusion, YOLO technology, as an efficient object detection algorithm, has shown great potential in the field of corrosion detection, particularly in marine and coastal engineering. However, the complexity of these environments and the challenge of obtaining high-quality annotated datasets make the annotation process laborious, potentially leading to model instability. Customized improvements, such as adjusting anchor box sizes, enhancing feature extraction networks, and improving loss functions, are necessary to address these issues. The accuracy of YOLO heavily depends on the quality and diversity of the training data, making it crucial to build a large-scale annotated dataset with various corrosion scenarios. In this study, focusing on corrosion issues in the southern coastal regions of China, 104 original data samples were collected and organized based on data from the National Center for Materials Corrosion and Protection Science of China. Through data augmentation techniques, a dataset of 1246 metal surface corrosion images were constructed, and an improved model based on YOLO v5 was established to identify and analyze the corrosion status of steel plates with different protective coatings, thereby providing technical support for rapid corrosion detection in metal structural facilities and assessing the performance of protective coatings in these regions.

2. Materials and Methods

This study first utilizes relevant data from the National Center for Materials Corrosion and Protection Science in China to construct a dataset of corrosion-marked images of various metal corrosion protection coatings using data processing techniques. Secondly, a new image recognition method (YOLO v5-GOLD-NWD) is proposed by improving upon the traditional YOLO v5. Furthermore, the proposed method is trained with the labeled image dataset for the identification of metal corrosion features, validating the feasibility of the proposed improvement method. Finally, based on the identification results of metal corrosion features, the protective effects of different metal corrosion protection coatings are evaluated, and corrosion coatings with better anticorrosive effects are recommended. Figure 1 depicts the basic research framework.
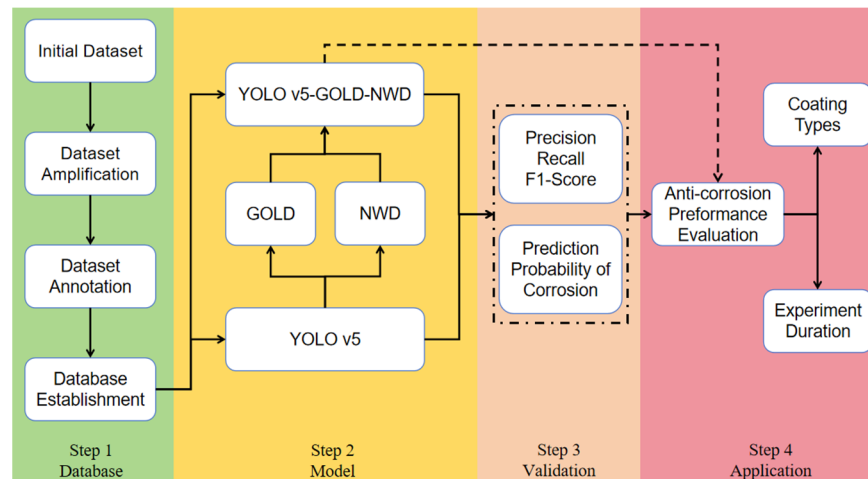
Figure 1. Research framework.

2.1. DATA

2.1.1. Dataset Collection

The dataset used in this study is sourced from the Natural Environment Corrosion Data (Experimental Station Corrosion Data) of the National Center for Materials Corrosion and Protection Science in China. This dataset encompasses various aspects such as corrosion test stations, environmental conditions, specimen materials, coating types, and test periods. Considering the completeness and clarity of data from various experimental stations, this study selected the metal corrosion detection dataset from the Zhoushan Seawater Station in Zhejiang, China (East China Sea). The environment at Zhoushan Seawater Station is extremely harsh, characterized by high salinity, high humidity, warm climate, and abundant marine life, all contributing to the rapid corrosion of metal materials. For the corrosion tests, the metal specimen material used is Q235 steel substrate with the dimensions of 100 mm in length, 50 mm in width, and 3 mm in thickness. The types of coatings include powder epoxy coating, epoxy coating, chlorinated rubber, fluorocarbon coating, and Wuxi anti-fouling coating. The basic information for the coated specimens is shown in Table 1.

Table 1. Basic information for different coatings.

Coating	Metal Substrate	Coating Composition	Total Coating Thickness
Powder epoxy coating	Q235 Steel	Powder Epoxy Coating (700 μm)	700 μm
Fluorocarbon coating	Q235 Steel	Epoxy Zinc-Rich Primer (70 μm)/Sealer/High-Build Epoxy Asphalt (300 μm)/Fluorocarbon Topcoat (60 μm)	430 μm
Epoxy coating	Q235 Steel	Inorganic Zinc-Rich Primer (70 μm)/Epoxy Mastic (150 μm)/Epoxy Topcoat (70 μm)	290 μm
Chlorinated rubber	Q235 Steel	Inorganic Zinc-Rich Primer (70 μm)/Sealer/Solvent-Free Ultra-High Build Epoxy Intermediate Coating (430 μm)	500 μm
Wuxi anti-fouling coating	Q235 Steel	Epoxy Zinc-Rich Primer (70 μm)/Epoxy Mastic (230 μm)/Wuxi Anti-Fouling Coating (150 μm)	450 μm

Considering that the metal sheet specimens suffer severe corrosion in this experimental environment, with almost the entire panel showing severe corrosion, this study focuses mainly on the metal sheet specimens with protective coatings as the analysis objects. During

the experiment, images of the specimens exposed outdoors for 24 and 60 months were recorded. A total of 104 valid image data points were obtained from these images as the initial dataset, as shown in Figure 2, which depicts an example of initial data samples.
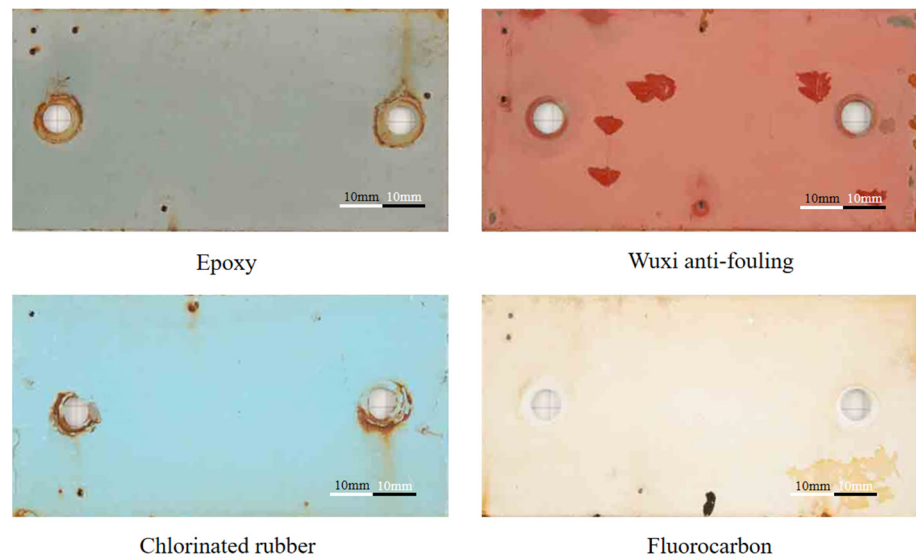

Epoxy

Wuxi anti-fouling

Chlorinated rubber

Fluorocarbon

Figure 2. Sample images in dataset.

2.1.2. Dataset Augmentation

Considering the limited size of the collected corrosion dataset, this study employs dataset augmentation techniques to expand the initial dataset. Common techniques for data augmentation include image cropping, rotation, flipping, scaling, horizontal mirroring, vertical mirroring, 90° rotation, 180° rotation, 270° rotation, pixel shifting, brightness adjustment, contrast adjustment, Gaussian noise addition, salt and pepper noise addition, etc. This study utilizes 11 data augmentation techniques as shown in Figure 3 to expand the initial dataset, generating a total of 1248 image dataset samples. During the data augmentation process, some augmented images exhibit anomalies, such as corrosion areas appearing at the edges of the images or corrosion features disappearing. Consequently, these images that do not meet the requirements are removed, resulting in a total of 1246 valid image dataset samples for training, validation, and testing of the model proposed in this study.
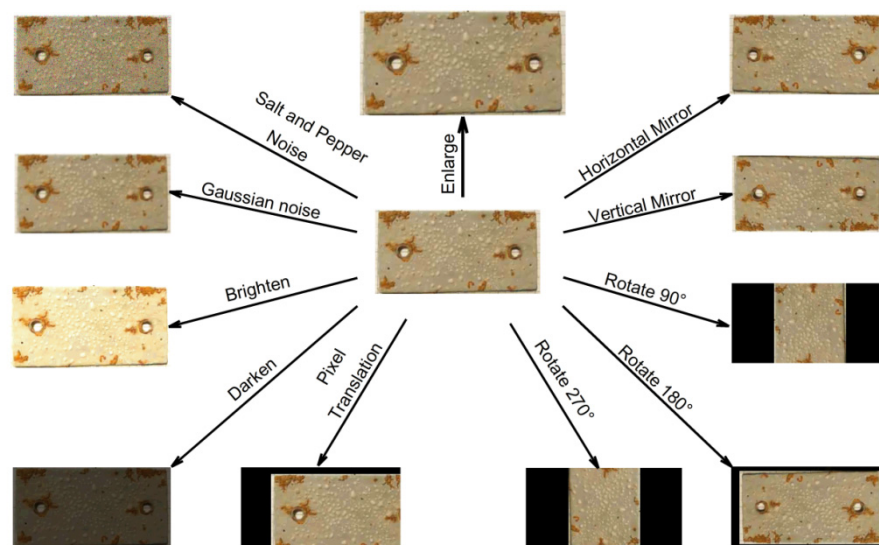

Figure 3. Data augmentation.

2.1.3. Image Annotation

Image annotation involves labeling the corrosion in images to create a dataset used for training machine learning models. It requires matching the corrosion labels of interest with the correct elements in the images. In this study, common types of metal corrosion were considered, and the image annotation software LabelImg (v1.8.1) was used to manually annotate the initial 104 images, forming the initial set of annotated image samples. Based on this, the weight parameters of this annotated sample set were obtained through model training. Subsequently, 1142 augmented images were automatically annotated using Python scripts. Finally, the automatically annotated data underwent manual inspection and fine-tuning to create the annotated image dataset used for model training.

2.2. YOLO v5-GOLD-NWD MODEL
2.2.1. Traditional YOLO v5 Model

The YOLO series algorithms have shown great potential in the field of object detection, especially with the introduction of YOLO v5, further promoting the widespread application of this algorithm. However, traditional YOLO v5 faces challenges such as limited generalization ability, high computational resource consumption, poor customization, and inadequate support from the development community [59]. Figure 4 depicts the framework structure of the traditional YOLO v5 model.
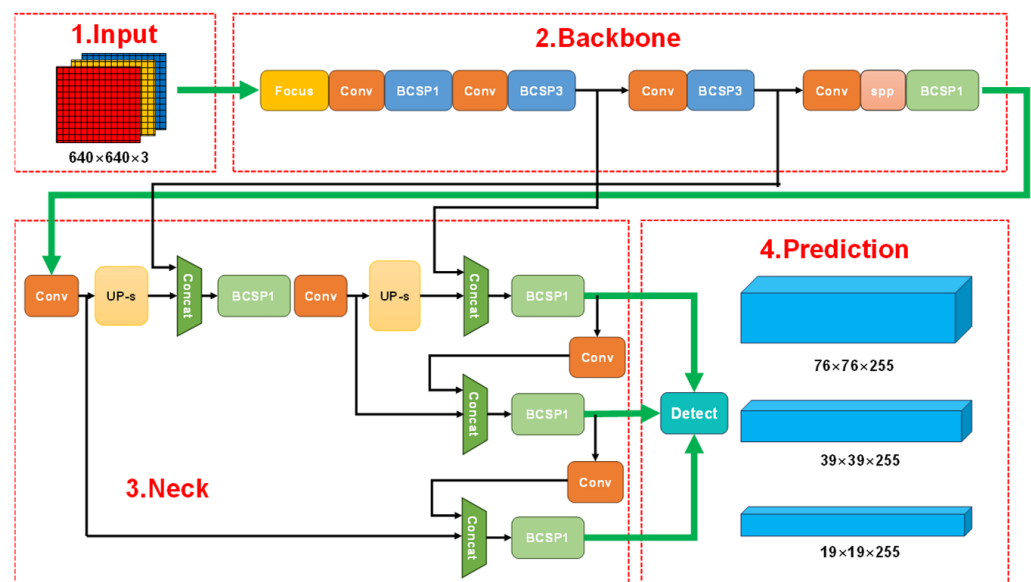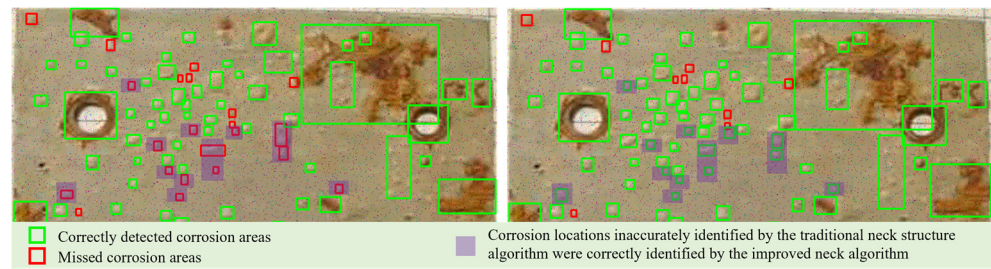

**Figure 4.** Framework structure of traditional YOLO v5.

The traditional YOLO v5 model utilizes the Feature Pyramid Network (FPN) to extract features from different levels and construct corresponding fusion structures. It merges the position information of small objects from low-level features with the position information of large objects from high-level features, thus compensating for the deficiencies in information at each level and enhancing the network's performance. However, the traditional FPN structure adopts a progressive information fusion mode, leading to information loss during cross-level fusion. During fusion, only the features of adjacent levels can be fully integrated, while obtaining information from other levels requires an indirect approach. As a result, cases of missed detections and false alarms are prone to occur, as shown in Figure 5.

Correctly detected corrosion areas
Missed corrosion areas
Corrosion locations inaccurately identified by the traditional neck structure algorithm were correctly identified by the improved neck algorithm

Figure 5. Corrosion recognition results based on traditional neck structure (**left**) and modified neck structure (**right**).

2.2.2. GOLD-YOLO Model

The typical approach to addressing the aforementioned issues often involves increasing the number of pathways to enhance information flow. Consequently, some improvements have been made to FPN structures by adding more pathways. However, this method encounters issues such as an excessive number of pathways and indirect interaction, leading to difficulties in cross-level information exchange and information loss. To overcome this challenge, this study refers to [60] and introduces a novel information interaction and fusion mechanism known as the gather-and-distribute Mechanism (GD). This mechanism is integrated into the GOLD-YOLO model framework, as illustrated in Figure 6. By globally aggregating features across different levels and injecting them into features at various levels, this framework achieves efficient information interaction and fusion. Without significantly increasing latency, the GD mechanism significantly enhances the information fusion capability of the Neck part of the model framework, thereby improving the model's detection capability for objects of different sizes.
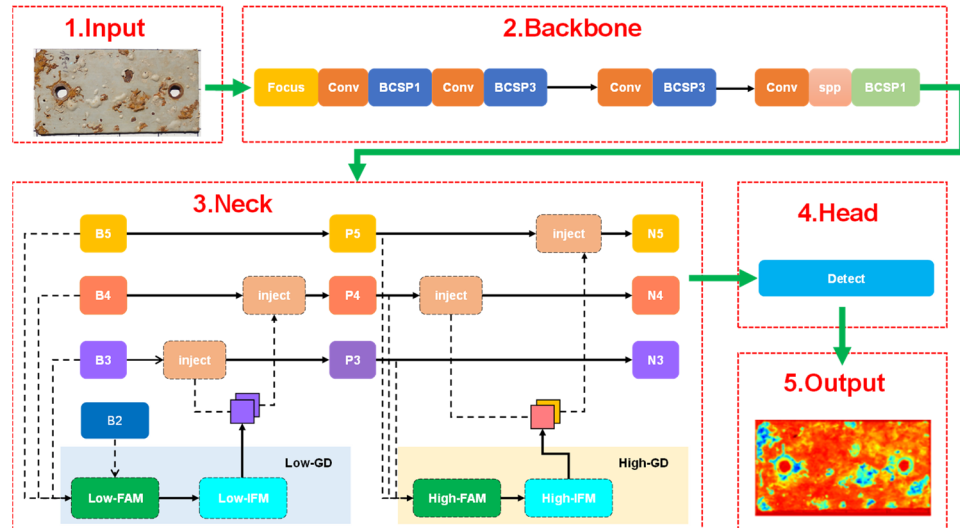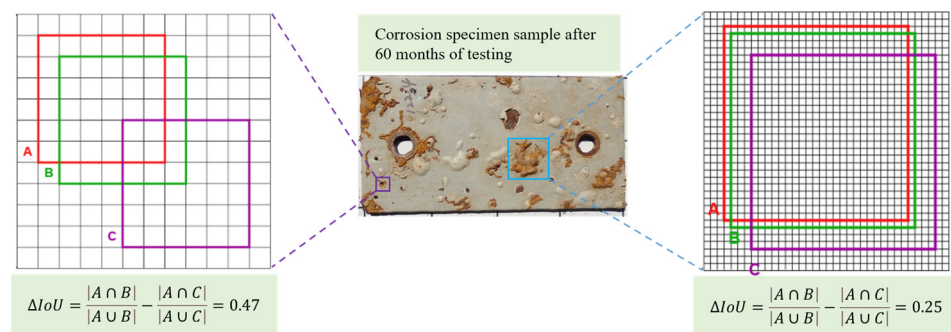

Figure 6. GOLD-YOLO Model Framework.

The GD mechanism consists of the Feature Alignment Module (FAM), Information Fusion Module (IFM), and Information Injection Module (Inject). The role of the Feature Alignment Module (FAM) is to collect features from different levels and align them, ensuring they have the same dimensions and semantic meanings. The Information Fusion Module (IFM) utilizes convolutional or Transformer operators to fuse the aligned features, generating a global feature representation. The Information Injection Module injects global feature information into different levels to ensure that each level benefits from global information, thereby improving the performance and effectiveness of the model.

To meet the detection requirements for objects of different sizes and balance the model's accuracy and speed, this study introduces two GD branches for information

fusion in GOLD-YOLO, namely the Low-GD branch and the High-GD branch. These two branches use convolutional and transformer operators to extract and fuse feature information, respectively. Additionally, considering that the corrosion areas in the image dataset of this study are mostly small-to-medium-sized targets, a gather-and-distribute mechanism is introduced in the model to enhance the detection capability for small targets, thereby improving the accurate identification of corrosion areas on metal specimens.

2.2.3. NWD Loss Function

The YOLO loss function typically employs Intersection over Union (IoU) to gauge the match between predicted bounding boxes and actual bounding boxes. However, as depicted in Figure 7, IoU exhibits significant sensitivity disparities for objects of different scales. For tiny objects (such as 6×6 pixels, left image), even slight position deviations in bounding boxes lead to a notable decrease in IoU, resulting in inaccurate label assignments. In contrast, for objects of normal size (such as 36×36 pixels, right image), the impact of bounding box position deviations on IoU reduction is relatively minor. The primary reason for this issue is that bounding box positions can only change discreetly, necessitating optimization of the bounding boxes.

$$\Delta IoU = \frac{|A \cap B|}{|A \cup B|} - \frac{|A \cap C|}{|A \cup C|} = 0.47 \qquad\qquad \Delta IoU = \frac{|A \cap B|}{|A \cup B|} - \frac{|A \cap C|}{|A \cup C|} = 0.25$$

Figure 7. Principle of loss function improvement: small object detection (**left**) and normal object detection (**right**).

In the original architecture of the YOLO v5 model, bounding box regression optimization typically relies on the Complete Intersection over Union (CIoU) loss function. The CIoU loss function combines Intersection over Union (IoU) of bounding boxes and the distance between their centers to mitigate potential localization instability caused by traditional IoU loss. While CIoU performs well in many object detection tasks, there is still room for improvement in its performance on small object detection. Small objects have a limited number of pixels, meaning even tiny localization errors could lead to significant fluctuations in IoU values, thereby affecting the overall performance of the model. Additionally, the performance of the CIoU loss function in emphasizing unique features of small objects is somewhat lacking, which may also contribute to its suboptimal performance in small object detection.

To address these issues, this study refers to [61] and adopts the Normalized Gaussian Wasserstein Distance (NWD) as the loss function in the GOLD-YOLO model. The NWD loss function models bounding boxes as Gaussian distributions and computes the Wasserstein distance between the two distributions to provide a more stable and balanced training process, thereby enhancing the model's performance in small object detection.

The core calculation formula of the *NWD* loss function is as described in Equation (1):

$$NWD(Q_a, Q_b) = exp\left(-\frac{\sqrt{W_2^2(Q_a, Q_b)}}{C}\right), \tag{1}$$

where Q_a and Q_b represent the Gaussian distribution parameters corresponding to two bounding boxes. This formula utilizes the square of the Wasserstein distance between

the two distributions to quantify the difference between two bounding boxes. *C* is a normalization constant used to adjust the sensitivity of the loss function, ensuring the stability of the training process. The calculation method is shown in Equation (2).

$$W_2^2(Q_a, Q_b) = \left\| \left(\left[c_{x_a}, c_{y_a}, \frac{\omega_a}{2}, \frac{h_a}{2} \right]^T, \left[c_{x_b}, c_{y_b}, \frac{\omega_b}{2}, \frac{h_b}{2} \right]^T \right) \right\|_2^2, \tag{2}$$

where c_{x_a}, c_{y_a} and c_{x_b}, c_{y_b} represent the coordinates of the centers of the two bounding boxes. $\omega_a, h_a, \omega_b,$ and h_b are the widths and heights of the two bounding boxes, respectively.

The NWD loss function not only optimizes the quantification of differences between bounding boxes but also effectively captures subtle features of small objects, thereby enhancing the model's accuracy in detecting small objects. Compared to the traditional CIoU loss function, NWD enhances the robustness and stability of the model against localization errors for small objects. It accurately captures the unique attributes of small objects, enhancing feature sensitivity. Additionally, by considering information from all targets in the image, it deepens the global understanding of the relationship between small objects and other objects. As a result, it improves the model's performance and precision in complex scenarios, especially providing effective recognition solutions for overlapping or occluded small objects. Furthermore, it enhances the adaptability and robustness of the model in handling such challenges. Therefore, based on the gather-and-distribute mechanism and NWD loss function, an improved YOLO v5-GOLD-NWD model is constructed for the identification and evaluation analysis of specific metal corrosion test image datasets in this study.

2.3. Model Evaluation Metrics

Precision, recall, F1 score, and confusion matrix are commonly used to evaluate the performance of machine learning models. This paper primarily employs these four metrics to assess the predictive accuracy of the model.

Precision refers to the proportion of true positive test boxes among all test boxes predicted as positive by the model. It reflects the model's ability to accurately predict positives. A high precision indicates that the model has a high proportion of true positives when predicting a particular class, and the model's false positive rate is relatively low. The calculation method is shown in Equation (3).

$$Precision = \frac{TP}{TP + FP} \tag{3}$$

where *TP* (True Positive) represents the number of positive samples correctly predicted by the model, and *FP* (False Positive) represents the number of negative samples incorrectly predicted as positive by the model.

Recall (or True Positive Rate) measures the proportion of all actual positive samples that the model correctly identifies, reflecting the model's ability to capture positive samples. A higher recall indicates that the model can effectively identify the most positive samples. The calculation formula for *Recall* is shown in Equation (4):

$$Recall = \frac{TP}{TP + FN} \tag{4}$$

where *FN* (False Negative) represents the number of actual positive samples that the model fails to identify.

F1 score, as the harmonic mean of precision and recall, provides a single measure that comprehensively considers both metrics. It evaluates the model's ability to balance precision and recall. Its calculation formula is as shown in Equation (5).

$$F1 - score = \frac{2 \times Precision \times Recall}{Precision + Recall} \tag{5}$$

The confusion matrix, represented as an $n \times n$ matrix, illustrates the correspondence between the model's predicted results and the actual categories, providing an effective tool for visual analysis of classification model performance. The confusion matrix reveals detailed information about the model's predictions, including correct predictions and various types of mispredictions, offering valuable insights for identifying prediction biases and optimizing model strategies.

2.4. Evaluation Method of Corrosion Resistance in Coatings

Analyses of anticorrosive performance were conducted based on acquired experimental data for the five coatings including powder epoxy coating, epoxy coating, chlorinated rubber, fluorocarbon coating, and Wuxi anti-fouling coating over different experimental periods (24 months and 60 months). Utilizing the YOLO v5-GOLD-NWD model, corrosion spots on coated metal plates were identified. The number of corrosion spots on each specimen was determined, and based on the identified corrosion spots, a statistical analysis was conducted to evaluate the protective effectiveness of each coating.

3. Results

3.1. Evaluation of Model Accuracy

To validate and evaluate the performance of the improved model, YOLO v5, YOLO v5-NWD, and YOLO v5-GOLD-NWD (the proposed model in this study) were selected for comparison and verification. The results indicate that YOLO v5-GOLD-NWD demonstrates superior recognition performance under the same training epochs (255 epochs). The metrics are summarized in Table 2, where it can be observed that YOLO v5-NWD shows improvements in precision, recall, F1 score, and predicted corrosion probability compared to the traditional YOLO v5 model, indicating the enhancement in metal corrosion recognition capability by introducing the NWD loss function. The precision of YOLO v5-GOLD-NWD model is 0.78, recall is 0.71, F1 score is 0.74, and predicted corrosion probability is 0.71, all of which are higher than the other two models. This indicates that the model performs better in metal corrosion recognition.

Table 2. Comparison of results among three models.

Model	Precision	Recall	F1 Score	Prediction Probability
YOLO v5	0.74	0.66	0.70	0.66
YOLO v5-NWD	0.74	0.69	0.72	0.69
YOLO v5-GOLD-NWD	0.78	0.71	0.74	0.71

Figure 8 illustrates the variation in prediction accuracy for the three models over training epochs. It can be observed that the proposed YOLO v5-GOLD-NWD model exhibits slightly lower precision in the initial stages compared to the other two models, and its convergence speed is slightly slower. However, after approximately 30 epochs of training, its precision steadily improves and stabilizes, achieving a 4% increase compared to both the YOLO v5 and YOLO v5-NWD models.

Figure 9 compares the confusion matrices of the three models. The traditional YOLO v5 model correctly identifies corrosion as corrosion with a probability of 0.66 and misidentifies the background as corrosion with a probability of 0.34. The YOLO v5-NWD model correctly identifies corrosion as corrosion with a probability of 0.69 and misidentifies the background as corrosion with a probability of 0.31. Meanwhile, the YOLO v5-GOLD-NWD model correctly identifies corrosion as corrosion with a probability of 0.71 and misidentifies the background as corrosion with a probability of 0.29. This demonstrates that YOLO v5-GOLD-NWD has better identification accuracy.
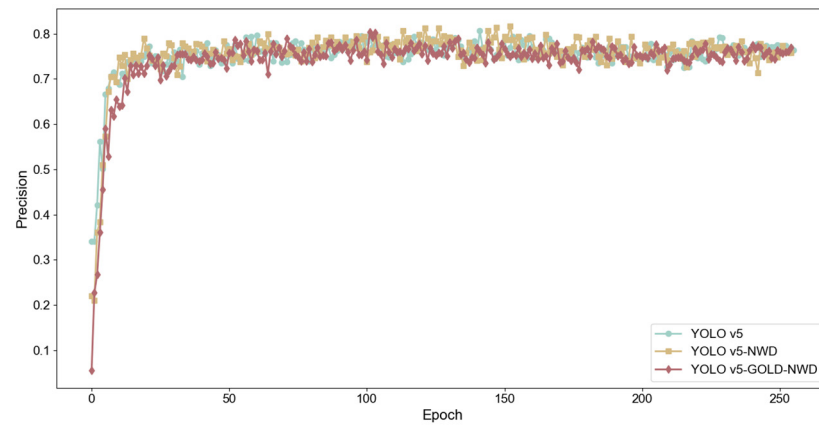
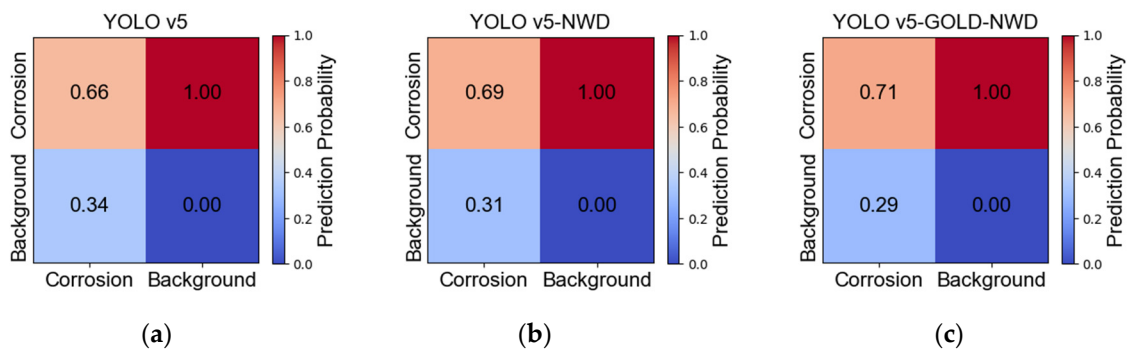**Figure 8.** Comparison of precision among three algorithms.

Figure 9. Confusion matrix results for the three models: (**a**) YOLO v5, (**b**) YOLO v5-NWD, and (**c**) YOLO v5-GOLD-NWD.

3.2. Evaluation of Corrosion Resistance in Coatings

The acquired corrosion image dataset mainly includes two test periods: 24 months and 60 months. Specifically, the data for the 24-month test period primarily consists of images of five types of coatings: powder epoxy coating, epoxy coating, chlorinated rubber, fluorocarbon coating, and Wuxi anti-fouling coating. Meanwhile, the data for the 60-month test period mainly comprise images of four types of coatings: powder epoxy coating, epoxy coating, chlorinated rubber, and fluorocarbon coating. To quantitatively evaluate the anti-corrosion performance of various coatings, a statistical analysis was conducted based on the recognition results of the corrosion image dataset (as shown in Table 3). The data were visualized using Kernel Density Estimation (KDE) [62] (as illustrated in Figure 10). Here, the KDE values reflect the density of data points surrounding the corrosion areas. In the figure, blue-green represents low density, indicating low frequency, while yellow-green represents high density, indicating high frequency. The dark blue areas indicate the boundary locations where corrosion occurs.

Table 3. Statistical results of corrosion spots for different coated specimens.

Metal Substrate	Coating	Symbols	Experimental Period (Months)	Number of Image Data	Number of Corrosion Spots
Q235 Steel	Powder epoxy coating	P	24	8	11
			60	14	19
	Fluorocarbon coating	F	24	8	28
			60	12	33
	Epoxy coating	E	24	16	162
			60	24	410
	Chlorinated rubber	C	24	2	21
			60	12	125
	Wuxi anti-fouling coating	W	24	8	129

(**a**) Powder Epoxy Coating (24 months)

(**a′**) Powder Epoxy Coating (60 months)

(**b**) Fluorocarbon Coating (24 months)

(**b′**) Fluorocarbon Coating (60 months)

(**c**) Epoxy Coating (24 months)

(**c′**) Epoxy Coating (60 months)

(**d**) Chlorinated Rubber Coating (24 months)

(**d′**) Chlorinated Rubber Coating (60 months)

(**e**) Wuxi Anti-fouling Coating (24 months)
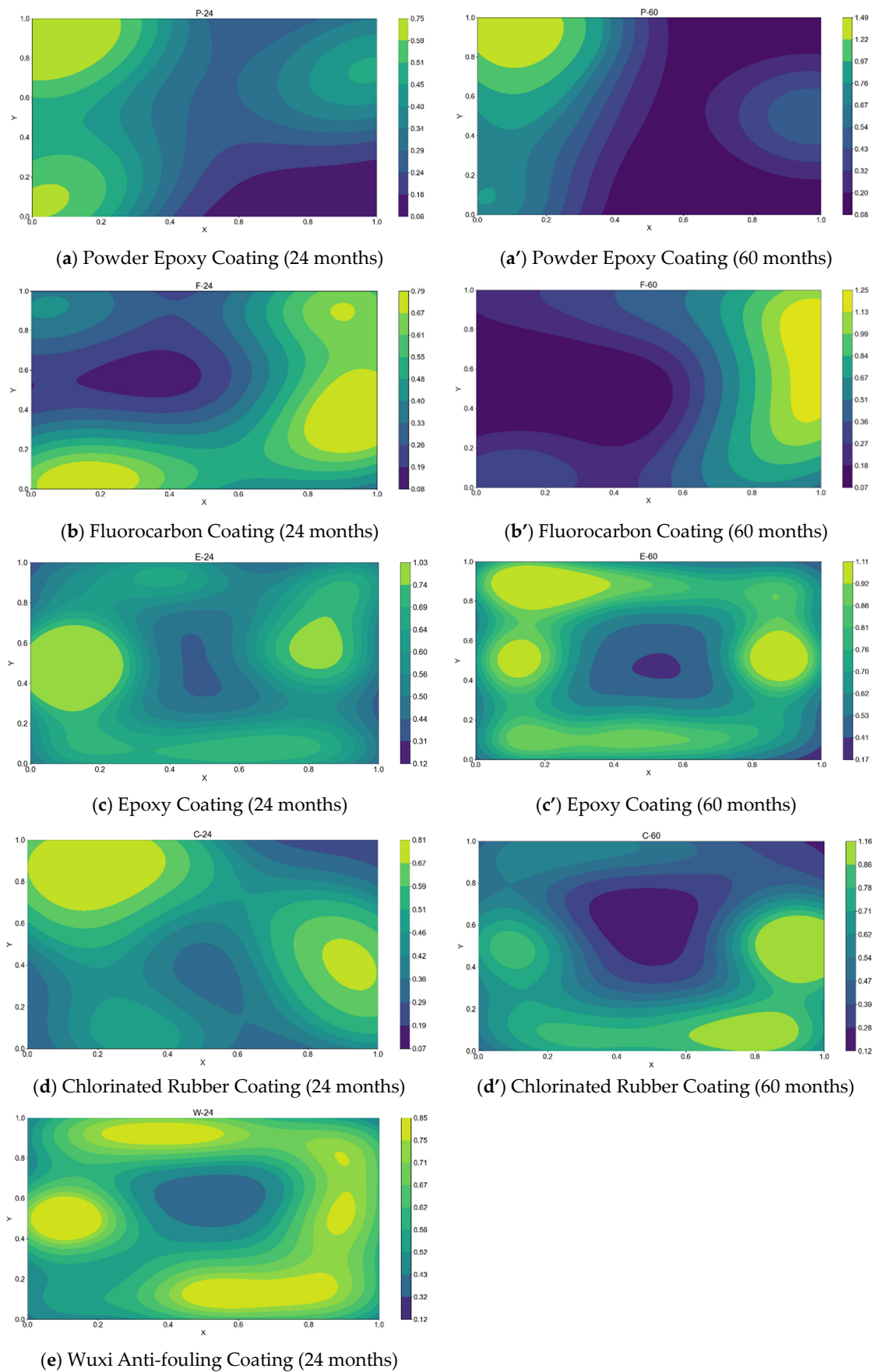
Figure 10. Corrosion distribution of different coated specimens during experimental periods.

From Figure 10(a,a'), it can be observed that the corrosion of the powder epoxy-coated samples primarily occurs in the upper left and lower left corners. The KDE value of the most severely corroded area reaches 0.75 at 24 months. This may be due to uneven coating on the edges. At 60 months, the most severe corrosion on the powder epoxy-coated metal samples is still concentrated in the upper left corner, with the KDE value reaching 1.49. There is also significant corrosion in the lower left corner, consistent with the 24-month observation but more severe. In addition, from Table 4, observations of the test samples show that most corrosion occurred at the corners within 24 and 60 months. Although the overall appearance of the samples did not change significantly, the location and progression of the corrosion over time were consistent with the identification results shown in Figure 10(a,a').
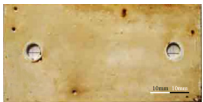
Table 4. Tested specimens at different months.
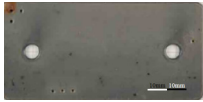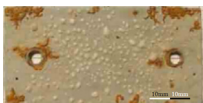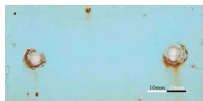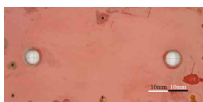
Coating	Tested Samples			
	24 Months	Appearance Description	60 Months	Appearance Description
P		No significant changes		No significant changes
F		Glossy, rust free, covered with 1–4 mm blisters		Glossy, rust free, covered with 1–3 mm blisters
E		No significant changes		There are many bubbles and a few small rust spots
C		No significant changes		Outer layer bulging, surface coating peeling off, with rust spots
W		There is a dissolved coating on the surface and slight corrosion		

Figure 10(b,b') show that, at 24 months, the corrosion of the fluorocarbon-coated samples is mainly concentrated around the fixed holes on the right side and lower left corner of the samples, with the most severe corrosion occurring on the fixing holes, showing a KDE value of 0.79. At 60 months, corrosion mainly occurs on the right side and upper right corner of the samples, with the most severe corroded area having a KDE value of 1.25. Overall, the corrosion worsens over time. In contrast, the corresponding tested specimens in Table 4 shows that the distribution of corrosion at 24 and 60 months is primarily on the right side and edges, which is consistent with the results based on the model, and also shows an increase in severity over time.

Figure 10(c,c') show that, at 24 months, the corrosion of the epoxy-coated samples is mainly around the fixed holes on both sides, with the most severe corrosion having a KDE value of 1.03. This is likely due to the edges where the coating application might be uneven and there is mechanical wear from fixing the samples. At 60 months, corrosion is mainly around the fixed holes on both sides and near the left upper edge, with the most severe corrosion showing a KDE value of 1.11. Compared to the 24-month results, the corrosion is more severe at 60 months. Additionally, the corresponding tested specimens in Table 4 shows that, at 24 months, corrosion mainly occurs around the two holes. At 60 months, corrosion spreads over the entire metal sheet, with rust spots around the holes and edges, and numerous blisters in the center, consistent with the results based on the model.

From Figure 10(d,d'), it can be observed that at 24 months, corrosion of the chlorinated rubber-coated samples mainly occurs in the upper left corner on the left side and around the fixed hole on the right side, with the most severe corrosion having a KDE value of 0.81. At 60 months, corrosion mainly occurs around the holes on the right side and bottom edge, with the most severe corrosion showing a KDE value of 1.15. There is also some corrosion accumulation around the holes on the left and upper left edge. Compared to the 24-month results, the corrosion distribution is similar at 60 months but with significantly increased severity. Additionally, the corresponding tested specimens in Table 4 show that, at 24 months, corrosion mainly occurs around the two holes and upper and lower edges, being relatively mild. At 60 months, corrosion is mainly around the holes but also appears on the edges, with some coating peeling off, matching well with the results based on the model.

From Figure 10e, it can be seen that, at 24 months, the corrosion of the anti-fouling-coated samples is relatively dispersed. Severe corrosion occurs around the fixed holes on both sides and near the top and bottom edges of the coating. The most severe corrosion shows a KDE value of 0.85. Additionally, the corresponding tested specimens in Table 4 show that corrosion mainly occurs around the metal sheet, with some coating peeling off, being relatively mild and matching the results based on the model.

Comparing the corrosion distribution of each specimen at 24 months, the results indicate that powder epoxy and chlorinated rubber coatings exhibit relatively good corrosion resistance, followed by epoxy coating, while the anti-fouling coating shows relatively poor protection. Comparing the corrosion distribution of each specimen at 60 months, the powder epoxy, fluorocarbon, and chlorinated rubber coatings have relatively small corrosion distribution areas, whereas the epoxy coating has a larger corrosion distribution. In terms of the concentration of corrosion sites, the probability of corrosion is highest in the powder epoxy-coated samples, followed by epoxy and chlorinated rubber coatings, with the fluorocarbon coating having the lowest probability. Therefore, in the early stages, powder epoxy, fluorocarbon, and chlorinated rubber coatings exhibit relatively good protective performance, while the anti-fouling coating shows poor protection. As the experimental period extends, powder epoxy and fluorocarbon coatings continue to demonstrate relatively better protective performance.

4. Discussion

Comparison with traditional YOLO v5 and YOLO v5-NWD models reveals that the image recognition performance of the proposed YOLO v5-GOLD-NWD model surpasses them in terms of precision, recall, and F1 score, indicating its superior recognition capability in image recognition. This also validates that improving the Neck structure and loss function of the traditional YOLO v5 model architecture can enhance detection accuracy. The Neck structure, typically situated between the Backbone and Head in neural networks, plays a role in feature fusion and enhancement. Introducing new attention mechanisms, skip connections, or multi-scale feature fusion techniques in the Neck structure can help the model better utilize features at different levels, thereby improving detection accuracy. Loss functions play a crucial role in training by measuring the difference between model predictions and true labels. For YOLO v5, the loss function can be enhanced through the introduction of new loss terms, adjustment of loss weights, or alteration of the loss calculation method. These modifications contribute to improved detection accuracy and overall model performance. However, the results indicate that the proposed improvement methods have only marginally enhanced the model's detection accuracy and performance. Further refinement is needed for improving the model, especially in the Neck structure and loss function enhancements. Additionally, the relatively low quantity and quality of image data used for model training are also significant factors limiting the improvement in detection accuracy and performance of the enhanced model.

Using the proposed improved model, corrosion image datasets of coated specimens were identified and statistically analyzed. After 24 months of environmental exposure,

corrosion points on specimens coated with powder epoxy, fluorocarbon, epoxy, and chlorinated rubber tended to be concentrated, primarily at the corners and around the fixing holes. In contrast, corrosion points on specimens with Wuxi anti-fouling coatings were more dispersed, showing significant corrosion except for the central part. After 60 months of exposure, corrosion points on specimens coated with powder epoxy, fluorocarbon, and chlorinated rubber remained concentrated, mainly at the corners and around the fixing holes. However, specimens with epoxy coatings showed significant diffusion of corrosion points compared to the 24-month period, indicating a noticeable decline in corrosion resistance after 60 months. In terms of the probability of corrosion occurrence, after 24 months of environmental exposure, specimens with epoxy coatings had the highest probability of corrosion, followed by Wuxi anti-fouling and chlorinated rubber coatings, while powder epoxy and fluorocarbon coatings had relatively lower probabilities. After 60 months of exposure, specimens with powder epoxy coatings had the highest probability of corrosion, followed by chlorinated rubber and epoxy coatings, while fluorocarbon coatings had the lowest probability. This suggests that the long-term corrosion resistance of powder epoxy coatings may be inadequate, while fluorocarbon coatings exhibited relatively good corrosion resistance at both 24 and 60 months of exposure. It is worth mentioning that the significantly poorer protective performance of the epoxy resin coating may be related to its relatively low thickness in the test specimen, which is approximately 290 μm.

The distribution of corrosion observed can be attributed to various factors, including the protective mechanisms and construction technology of the coatings. Powder epoxy coatings primarily provide corrosion protection through physical barrier mechanisms. These coatings form a hard protective layer that effectively prevents the penetration of moisture, oxygen, and other corrosive agents, thereby slowing down the corrosion rate of the substrate. Fluorocarbon coatings exhibit excellent chemical corrosion resistance and weather resistance. They mainly prevent chemical substances and water penetration through their very low surface energy and inert surface, thereby providing corrosion protection. Epoxy coatings typically have good adhesion and chemical corrosion resistance. They mainly prevent erosion from oxygen, moisture, and other corrosive media on the substrate by forming a dense, sturdy protective film. Chlorinated rubber coatings possess good chemical corrosion resistance and weather resistance. They primarily prevent corrosion media from erosion through their dense structure and chemical stability. Wuxi anti-fouling coatings usually contain organosilicon and other special additives, forming a dense, uniform coating layer that prevents the penetration of moisture, chemicals, and pollutants, thereby providing corrosion and fouling protection.

From the perspective of corrosion protection mechanisms, all types of coatings should exhibit good corrosion resistance during the test period. However, the corrosion protection mechanisms of powder epoxy coatings, epoxy coatings, and Wuxi anti-fouling coatings all involve the formation of a dense, uniform protective film to prevent moisture, oxygen, and other corrosive media from eroding the substrate. Once defects occur in the coatings, it can greatly reduce their corrosion resistance and may lead to rapid corrosion evolution. During the experimental process, coatings may inevitably exhibit various degrees of deficiencies, such as uneven coating implementation, coating fracture or cracking, improper surface treatment of the metal, electrolytic corrosion, etc. Especially at the edges of the specimens, coating defects are more likely to occur. For instance, at the edges and corners of specimens, uneven coating implementation may lead to insufficient coating thickness or coating defects, exposing the metal to corrosion. Additionally, stress concentration at the edges and corners of specimens may cause coating fracture or cracking, exposing the metal surface to environmental corrosion. Furthermore, the reasons for the above results are also related to the quantity and quality of the collected original image data. Particularly when the quantity is insufficient, the model training samples may be inadequate, leading to deviations in the model's detection results. For example, in the 24-month natural exposure test, the original image data for the specimens with four types of coatings were fewer than 10

images. This insufficient data for model training may result in non-generalizable model recognition results.

5. Conclusions

Coastal areas face severe corrosion issues, posing significant risks and economic losses to equipment, personnel, and the environment. With technological advancements, machine vision techniques have been widely employed in the detection and identification of metal corrosion to enhance detection accuracy and reduce maintenance costs. This study proposes an improved YOLO v5-GOLD-NWD model architecture and trains it using corrosion data from the National Center for Materials Corrosion and Protection Science in China. A comparison with the traditional YOLO v5 and the improved YOLO v5-NWD models reveals that the proposed YOLO v5-GOLD-NWD model outperforms in detection accuracy, achieving a precision rate of 78%, a 4% improvement over the traditional YOLO v5 models. The YOLO v5-GOLD-NWD model proposed in this paper performs effectively in water corrosion detection, especially for the Zhoushan seawater station samples described in this study.

This study reveals that, in terms of the probability of corrosion occurrence, specimens with epoxy coatings had the highest probability after 24 months, followed by Wuxi anti-fouling and chlorinated rubber coatings, with powder epoxy and fluorocarbon coatings having relatively lower probabilities. After 60 months, specimens with powder epoxy coatings exhibited the highest probability of corrosion, followed by chlorinated rubber and epoxy coatings, while fluorocarbon coatings had the lowest probability, suggesting superior long-term corrosion resistance. Overall, in the corrosive environment where Zhoushan Seawater Station is located, fluorocarbon coatings prove to be the most effective for long-term corrosion protection, while other coatings may falter under prolonged exposure. Powder epoxy coatings, initially resilient, show degradation over time, limiting their suitability for extended corrosion protection. Epoxy coatings, though widely used, exhibit significant deterioration, particularly after 60 months, potentially compromising long-term protection. Chlorinated rubber coatings, while moderately effective initially, demonstrate increasing corrosion severity over time compared to fluorocarbon coatings, indicating limitations in long-term performance. The Wuxi anti-fouling coating, while initially dispersing corrosion points, exhibits significant corrosion, except in the central part, suggesting inferior corrosion resistance. Hence, it may not be ideal for applications requiring robust and durable corrosion protection. In summary, the long-term corrosion resistance of the coatings mentioned in this study rank as follows: fluorocarbon, powder epoxy, chlorinated rubber, epoxy, and Wuxi anti-fouling. It is worthy to note that the epoxy coating, with a thinner thickness of 290 μm compared to other coatings, might exhibit more significant corrosion effects.

Despite the improved accuracy in metal corrosion detection demonstrated by the proposed model compared to traditional YOLO v5 and YOLO v5 NWD models, several limitations remain. The dataset's quality and quantity constrain further comprehensive validation and optimization of the model. Enhancing the model's robustness and generalization capabilities is necessary to tackle corrosion detection tasks under varying environmental conditions and complex scenarios. Additionally, the evaluation of coating corrosion resistance may lack universality due to insufficient data samples, and this study does not extensively discuss the long-term performance (beyond 60 months) of some coatings, potentially affecting the comprehensive assessment of their effectiveness. Future research will address these limitations by expanding the dataset and conducting extensive field testing to validate and refine the model's practicality and reliability. These efforts aim to improve metal corrosion detection accuracy and provide effective corrosion protection solutions across various environments, advancing the field's technological progress and application development.

References

1. Abbas, M.; Shafiee, M. An overview of maintenance management strategies for corroded steel structures in extreme marine environments. *Mar. Struct.* **2020**, *71*, 102718. [CrossRef]
2. Lei, Y.; Sheng, N.; Ohtsuka, T. *Corrosion and Protection of Marine Engineering Materials*; China-South Asia STM Publishing Center: New Delhi, India, 2021.
3. Chandler, K.A. *Marine and Offshore Corrosion: Marine Engineering Series*; Elsevier: Amsterdam, The Netherlands, 2014.
4. James, A.; Bazarchi, E.; Chiniforush, A.A.; Aghdam, P.P.; Hosseini, M.R.; Akbarnezhad, A.; Martek, I.; Ghodoosi, F. Rebar corrosion detection, protection, and rehabilitation of reinforced concrete structures in coastal environments: A review. *Constr. Build. Mater.* **2019**, *224*, 1026–1039. [CrossRef]
5. Neocleous, K.; Christofe, A.; Agapiou, A.; Evagorou, E.; Themistocleous, K.; Hadjimitsis, D. Digital mapping of corrosion risk in coastal urban areas using remote sensing and structural condition assessment: Case study in Cyprus. *Open Geosci.* **2016**, *8*, 662–674. [CrossRef]
6. Hu, J.; Zhang, S.; Chen, E.; Li, W. A review on corrosion detection and protection of existing reinforced concrete (RC) structures. *Constr. Build. Mater.* **2022**, *325*, 126718. [CrossRef]
7. Imran, M.M.H.; Jamaludin, S.; Ayob, A.F.M.; Ali, A.A.I.M.; Ahmad, S.Z.A.S.; Akhbar, M.F.A.; Suhrab, M.I.R.; Zainal, N.; Norzeli, S.M.; Mohamed, S.B. Application of artificial intelligence in marine corrosion prediction and detection. *J. Mar. Sci. Eng.* **2023**, *11*, 256. [CrossRef]
8. Lin, Z.; Zhang, W.; Li, J.; Yang, J.; Han, B.; Xie, P. Application of artificial intelligence (AI) in the area of corrosion protection. *Anti-Corros. Methods Mater.* **2023**, *70*, 243–251. [CrossRef]
9. Ali, A.A.I.M.; Jamaludin, S.; Imran, M.M.H.; Ayob, A.F.M.; Ahmad, S.Z.A.S.; Akhbar, M.F.A.; Suhrab, M.I.R.; Ramli, M.R. Computer Vision and Image Processing Approaches for Corrosion Detection. *J. Mar. Sci. Eng.* **2023**, *11*, 1954. [CrossRef]
10. Jiao, P.; Ye, X.; Zhang, C.; Li, W.; Wang, H. Vision-based real-time marine and offshore structural health monitoring system using underwater robots. *Comput.-Aided Civ. Infrastruct. Eng.* **2024**, *39*, 281–299. [CrossRef]
11. Panda, J.P. Machine learning for naval architecture, ocean and marine engineering. *J. Mar. Sci. Technol.* **2023**, *28*, 1–26. [CrossRef]
12. Idris, S.A.; Jafar, F.A. Image enhancement based on software filter optimization for corrosion inspection. In Proceedings of the 2014 5th International Conference on Intelligent Systems, Modelling and Simulation, Langkawi, Malaysia, 27–29 January 2014.
13. Son, H.; Hwang, N.; Kim, C.; Kim, C. Rapid and automated determination of rusted surface areas of a steel bridge for robotic maintenance systems. *Autom. Constr.* **2014**, *42*, 13–24. [CrossRef]
14. Jahanshahi, M.R.; Masri, S.F. Parametric performance evaluation of wavelet-based corrosion detection algorithms for condition assessment of civil infrastructure systems. *J. Comput. Civil Eng.* **2013**, *27*, 345–357. [CrossRef]
15. Chen, P.H.; Shen, H.K.; Lei, C.Y.; Chang, L.M. Fourier-transform-based method for automated steel bridge coating defect recognition. *Proc. Eng.* **2011**, *14*, 470–476. [CrossRef]
16. Khayatazad, M.; De Pue, L.; De Waele, W. Detection of corrosion on steel structures using automated image processing. *Dev. Built Environ.* **2020**, *3*, 100022. [CrossRef]
17. Xia, D.-H.; Song, S.; Tao, L.; Qin, Z.; Wu, Z.; Gao, Z.; Wang, J.; Hu, W.; Behnamian, Y.; Luo, J.-L. Review-material degradation assessed by digital image processing: Fundamentals, progresses, and challenges. *J. Mater. Sci. Technol.* **2020**, *53*, 146–162. [CrossRef]
18. Bishop, C.M. *Pattern Recognition and Machine Learning*; Springer: Berlin/Heidelberg, Germany, 2006; pp. 645–678.
19. Vapnik, V.N. An overview of statistical learning theory. *IEEE Trans. Neural Netw.* **1999**, *10*, 988–999. [CrossRef] [PubMed]
20. Ahuja, S.K.; Shukla, M.K. A survey of computer vision-based corrosion detection approaches. In *Information and Communication Technology for Intelligent Systems (ICTIS 2017)*; Kumar, S., Manoj, A., Shukla, K., Eds.; Springer International Publishing AG: Ahmedabad, India, 2018; Volume 2, pp. 55–63.

21. Atha, D.J.; Jahanshahi, M.R. Evaluation of deep learning approaches based on convolutional neural networks for corrosion detection. *Struct. Health Monit.* **2018**, *17*, 1110–1128. [CrossRef]

22. Forkan, A.R.M.; Kang, Y.-B.; Jayaraman, P.P.; Liao, K.; Kaul, R.; Morgan, G.; Ranjan, R.; Sinha, S. CorrDetector: A framework for structural corrosion detection from drone images using ensemble deep learning. *Expert Syst. Appl.* **2022**, *193*, 116461. [CrossRef]

23. Cha, Y.J.; Choi, W.; Suh, G.; Mahmoudkhani, S.; Büyüköztürk, O. Autonomous structural visual inspection using region-based deep learning for detecting multiple damage types. *Comput.-Aided Civ. Infrastruct. Eng.* **2018**, *33*, 731–747. [CrossRef]

24. Yao, Y.; Liu, G.J.; Li, S.Z.; Liu, M.; Chen, C.; Huang, T.; Lin, H.; Li, Z.; Liu, Y.; Wang, Z. Research Progress on Corrosion Prediction Model of Metallic Materials for Electrical Equipment. *J. Chin. Soc. Corros. Prot.* **2023**, *43*, 983–991. (In Chinese)

25. Kordijazi, A.; Zhao, T.; Zhang, J.; Alrfou, K.; Rohatgi, P. A review of application of machine learning in design, synthesis, and characterization of metal matrix composites: Current status and emerging applications. *JOM* **2021**, *73*, 2060–2074. [CrossRef]

26. Wang, H.T.; Han, E.-H.; Ke, W. Artificial neural network modeling for atmospheric corrosion of carbon steel and low alloy steel. *Corros. Sci. Prot. Technol.* **2006**, *18*, 144. (In Chinese)

27. Hua, G.R.; Li, W.H.; Guo, Y.Y. Corrosion rate prediction of Q235 steel in Hainan substation grounding grid based on neural network models. *Corros. Prot.* **2017**, *38*, 573. (In Chinese)

28. Zhao, L.; Luo, Z.; Deng, G.; Shi, V. Prediction of corrosion failure probability of buried oil and gas pipeline based on an RBF neural network. *Front. Earth Sci.* **2023**, *11*, 1148407. [CrossRef]

29. Lu, H.; Peng, H.; Xu, Z.D.; Matthews, J.C.; Wang, N.; Iseley, T. A feature selection–based intelligent framework for predicting maximum depth of corroded pipeline defects. *J. Perform. Constr. Facil.* **2022**, *36*, 04022044. [CrossRef]

30. Komijani, H.; Rezaeihassanabadi, S.; Parsaei, M.R.; Maleki, S. Radial basis function neural network for electrochemical impedance prediction at presence of corrosion inhibitor. *Period. Polytech. Chem. Eng.* **2017**, *61*, 128–132. [CrossRef]

31. Liu, S.; Liu, H.; Liu, Z. Quantification of pitting corrosion from thermography using deep neural networks. *Rev. Sci. Instrum.* **2021**, *92*, 035116. [CrossRef]

32. Bastian, B.T.; Jaspreeth, N.; Ranjith, S.K.; Jiji, C.V. Visual inspection and characterization of external corrosion in pipelines using deep neural network. *NDT&E Int.* **2019**, *107*, 102134.

33. Luo, W.; Liu, T.; Li, W.; Luo, M. Pitting corrosion prediction based on electromechanical impedance and convolutional neural networks. *Struct. Health Monit.* **2023**, *22*, 1647–1664. [CrossRef]

34. Idusuyi, N.; Samuel, O.J.; Olugasa, T.T.; Ajide, O.O.; Abu, R. Corrosion modelling using convolutional neural networks: A brief overview. *J. Bio-Tribo-Corros.* **2022**, *8*, 72. [CrossRef]

35. Halama, M.; Kreislova, K.; Van Lysebettens, J. Prediction of atmospheric corrosion of carbon steel using artificial neural network model in local geographical regions. *Corrosion* **2011**, *67*, 065004-1. [CrossRef]

36. Wang, H.; Han, E.; Ke, W. Predictive model for atmospheric corrosion of aluminium alloy by artificial neural network. *J. Chin. Soc. Corros. Prot.* **2006**, *26*, 272–274. (In Chinese)

37. Jin, H.; Wang, M.; Xiang, H.; Liu, X.; Wang, C.; Fu, D. A PSO-RBF prediction method on flow corrosion of heat exchanger using the industrial operations data. *Process Saf. Environ. Prot.* **2024**, *183*, 11–23. [CrossRef]

38. Yang, X.; Jia, L.; Meng, Q. A quantitative detection method for stress corrosion cracks in turbine discs using a BPSO-RBFNN model. *Meas. Sci. Technol.* **2018**, *29*, 095014. [CrossRef]

39. Zhang, S.; Deng, X.; Lu, Y.; Hong, S.; Kong, Z.; Peng, Y.; Luo, Y. A channel attention based deep neural network for automatic metallic corrosion detection. *J. Build. Eng.* **2021**, *42*, 103046. [CrossRef]

40. Barile, C.; Casavola, C.; Pappalettera, G.; Kannan, V.P. Designing a deep neural network for an acousto-ultrasonic investigation on the corrosion behaviour of CORTEN steel. *Proc. Struct. Integr.* **2022**, *37*, 307–313. [CrossRef]

41. Andersen, R.; Nalpantidis, L.; Ravn, O.; Boukas, E. Investigating deep learning architectures towards autonomous inspection for marine classification. In Proceedings of the 2020 IEEE International Symposium on Safety, Security, and Rescue Robotics (SSRR), Abu Dhabi, United Arab Emirates, 4–6 November 2020.

42. Yao, Y.; Yang, Y.; Wang, Y.; Zhao, X. Artificial intelligence-based hull structural plate corrosion damage detection and recognition using convolutional neural network. *Appl. Ocean Res.* **2019**, *90*, 101823. [CrossRef]

43. Holm, E.; Transeth, A.A.; Knudsen, O.Ø.; Stahl, A. Classification of corrosion and coating damages on bridge constructions from images using convolutional neural networks. In Proceedings of the Twelfth International Conference on Machine Vision (ICMV 2019), Amsterdam, The Netherlands, 16–18 November 2019.

44. Zhi, Y.; Fu, D.; Zhang, D.; Yang, T.; Li, X. Prediction and Knowledge Mining of Outdoor Atmospheric Corrosion Rates of Low Alloy Steels Based on the Random Forests Approach. *Metals* **2019**, *9*, 383. [CrossRef]

45. Xinsheng, Z.; Baoquan, C. Corrosion prediction of submarine pipelines based on improved random forest model. *China Saf. Sci. J.* **2021**, *31*, 69.

46. Diao, Y.; Yan, L.; Gao, K. Improvement of the machine learning-based corrosion rate prediction model through the optimization of input features. *Mater. Des.* **2021**, *198*, 109326. [CrossRef]

47. Yan, L.; Diao, Y.; Lang, Z.; Gao, K. Corrosion rate prediction and influencing factors evaluation of low-alloy steels in marine atmosphere using machine learning approach. *Sci. Technol. Adv. Mater.* **2020**, *21*, 359–370. [CrossRef]

48. Li, Q.; Xia, X.; Pei, Z.; Cheng, X.; Zhang, D.; Xiao, K.; Wu, J.; Li, X. Long-term corrosion monitoring of carbon steels and environmental correlation analysis via the random forest method. *Npj Mater. Degrad.* **2022**, *6*, 1. [CrossRef]

49. Li, Q.; Wang, J.; Wang, K.; Yuan, J.; Xing, X.; Liu, X.; Hu, W. Determination of corrosion types from electrochemical noise by gradient boosting decision tree method. *Int. J. Electrochem. Sci.* **2019**, *14*, 1516–1528. [CrossRef]

50. Fang, S.F.; Wang, M.P.; Qi, W.H.; Zheng, F. Hybrid genetic algorithms and support vector regression in forecasting atmospheric corrosion of metallic materials. *Comput. Mater. Sci.* **2008**, *44*, 647–655. [CrossRef]

51. Lv, Y.J.; Wang, J.W.; Wang, J.; Xiong, C.; Zou, L.; Li, L.; Li, D.W. Steel corrosion prediction based on support vector machines. *Chaos Solitons Fractals* **2020**, *136*, 109807. [CrossRef]

52. Zhang, W.D.; Shen, B.; Ai, Y.B.; Yang, B. Gas pipeline corrosion prediction based on modified support vector machine and unequal interval model. *Appl. Mech. Mater.* **2013**, *373*, 1987–1994. [CrossRef]

53. Chen, P.H.; Shen, H.K.; Lei, C.Y.; Chang, L.M. Support-vector-machine-based method for automated steel bridge rust assessment. *Autom. Constr.* **2012**, *23*, 9–19. [CrossRef]

54. Redmon, J.; Divvala, S.; Girshick, R.; Farhadi, A. You only look once: Unified, real-time object detection. In Proceedings of the IEEE Conference on Computer Vision and Pattern Recognition, Las Vegas, NV, USA, 26 June–1 July 2016.

55. Jia, Z.; Fu, M.; Zhao, X.; Cui, Z. Intelligent identification of metal corrosion based on Corrosion-YOLOv5s. *Displays* **2023**, *76*, 102367. [CrossRef]

56. Zhang, D.Y.; Wei, P.H.; Tan, M.W.; Chen, C.; Wang, L.; Hong, W. Investigation of aircraft surface defects detection based on YOLO neural network. In Proceedings of the 2020 7th International Conference on Information Science and Control Engineering (ICISCE), Changsha, China, 18–20 December 2020.

57. Nabizadeh, E.; Parghi, A. Automated corrosion detection using deep learning and computer vision. *Asian J. Civ. Eng.* **2023**, *24*, 2911–2923. [CrossRef]

58. Ameli, Z.; Nesheli, S.J.; Landis, E.N. Deep Learning-Based Steel Bridge Corrosion Segmentation and Condition Rating Using Mask RCNN and YOLOv8. *Infrastructures* **2023**, *9*, 3. [CrossRef]

59. Jocher, G.; Nishimura, K.; Mineeva, T.; Vilariño, R. YOLOv5; GitHub Repository. 2020. Available online: https://github.com/ultralytics/yolov5 (accessed on 15 May 2024).

60. Wang, C.; He, W.; Nie, Y.; Guo, J.; Liu, C.; Wang, Y.; Han, K. Gold-YOLO: Efficient object detector via gather-and-distribute mechanism. In Proceedings of the NeurIPS Proceedings 2023, New Orleans, LA, USA, 10–16 December 2023.

61. Wang, J.; Xu, C.; Yang, W.; Yu, L. A normalized Gaussian Wasserstein distance for tiny object detection. *arXiv* **2021**, arXiv:2110.13389.

62. Heer, J. Fast & Accurate Gaussian Kernel Density Estimation. In Proceedings of the 2021 IEEE Visualization Conference (VIS), New Orleans, LA, USA, 24–29 October 2021.